Available online at www.sciencedirect.com
SCIENCE DIRECT®
Journal of Sound and Vibration 279 (2005) 253–274
JOURNAL OF SOUND AND VIBRATION
www.elsevier.com/locate/jsvi

Optimum parameters of Maxwell model-defined dampers used to link adjacent structures

H.P. Zhu[a], Y.L. Xu[b,*]

[a] School of Civil Engineering & Mechanics, Huazhong University of Science & Technology, 430074 Wuhan, China
[b] Department of Civil & Structural Engineering, The Hongkong Polytechnic University, Kowloon, Hong Kong, China

Received 14 February 2003; accepted 31 October 2003

Abstract

The analytical formulas for determining optimum parameters of Maxwell model-defined fluid dampers used to link two adjacent structures are derived in this paper using the principle of minimizing the averaged vibration energy of either the primary structure or the two adjacent structures under a white-noise ground excitation. Each structure is modelled as a single-degree-of-freedom system, which is connected to the other structure through a Maxwell model-defined fluid damper. The derived formulas explicitly express the optimum parameters of the fluid damper, i.e., the relaxation time and the damping coefficient at zero frequency, as the functions of the frequency and mass ratios of two adjacent structures. The dynamic analysis shows that the fluid damper of optimum parameters can significantly reduce the dynamic responses of most adjacent structures under the white-noise ground excitation. The fluid damper of optimum parameters is then applied to the adjacent structures subjected to either a filtered white-noise ground excitation or the El Centro 1940 NS ground excitation. The results demonstrate that the fluid damper of optimum parameters derived based on the white-noise ground excitation is also beneficial to reduce the responses of the adjacent structures under the filtered white-noise ground excitation and the El Centro ground excitation.

1. Introduction

The possibility of using active or passive control devices to link adjacent structures has been explored in recent decades. This approach takes advantage of the interaction between adjacent structures, which is expected not only to overcome the problem of pounding between adjacent structures but also to reduce the seismic or wind-induced responses of the adjacent structures if the parameters of control devices are selected properly. Gurley et al. [1] considered two uniform

*Corresponding author. Tel.: +852-27666050; fax: +852-23346389.
E-mail addresses: hpzhu@hust.edu.cn (H.P. Zhu), ceylxu@polyu.edu.hk (Y.L. Xu).

0022-460X/$ - see front matter © 2003 Elsevier Ltd. All rights reserved.
doi:10.1016/j.jsv.2003.10.035

shear beams, representing two adjacent tall buildings, linked by a Voigt model-defined damper against wind excitation. The beneficial stiffness and damping ratio of the Voigt model-defined viscoelastic damper were then found through extensive numerical parametric studies in terms of the minimization of the peak amplitude of the response transfer function of the primary structure under harmonic excitation. Luco and De Barros [2] used the same shear beam models and optimum principle as used by Gurley et al. [1] to investigate the optimum distribution of the Voigt model-defined viscoelastic dampers against earthquake excitation. The optimum damper ratios were determined for a class of adjacent structures with different heights and floor masses. Iwanami et al. [3] carried out an analytical study and found the optimum damping ratio and stiffness of the Voigt model-defined damper linking two adjacent buildings for the particular case $m_1k_1 = m_2k_2$ by assuming each of the linked structures as a single-degree-of-freedom system. Zhang and Xu [4] performed the numerical investigations of dynamic characteristics and seismic responses of two adjacent structures linked by discrete viscoelastic dampers. They identified the optimum parameters of the Voigt model-defined dampers by maximizing the modal damping ratios through extensive numerical parametric studies.

All the above studies to find the optimum parameters of the Voigt model-defined dampers linking two adjacent structures, however, were carried out for specific adjacent structures, and no analytical formulas for the optimum parameters of dampers were provided. From a practical use of viewpoint, it is better to provide general analytical formulas to facilitate the engineers' selection of the optimum parameters of dampers linking two adjacent structures as what has been done for the tuned mass dampers by Warburton [5] and for mega-substructure systems by Feng and Mita [6]. To this end, Zhu and Iemura [7] modelled two adjacent structures as two single-degree-of-freedom (s.d.o.f.) systems and derived the general analytical formulas for the optimum stiffness and damping ratio of the Voigt model-defined damper connecting two s.d.o.f. systems subjected to a white-noise ground excitation.

In recent years, the Maxwell model-defined fluid dampers have found many applications, such as those described by Constantinou and Symans [8] and Soong and Dargush [9], in mitigating wind- or seismic-induced response of large civil structures. The Maxwell model-defined fluid dampers have also been proposed to link adjacent buildings against earthquake excitation by Zhang and Xu [10]. They obtained the beneficial damper relaxation time and damping coefficient at zero frequency for achieving the maximum modal damping ratios and the maximum seismic response reduction of two shear buildings through numerical parametric studies. However, no general analytical formulas were given for the optimum parameters of fluid dampers connecting two adjacent buildings.

This study thus aims to derive the analytical formulas for the optimum relaxation time and damping coefficient at zero frequency of the Maxwell model-defined fluid dampers connecting two adjacent structures. Each structure is modelled as a single-degree-of-freedom system, which is connected to the other structure through the Maxwell model-defined fluid damper. The optimum parameters of the fluid damper are determined by minimizing the averaged vibration energy of either the primary structure or the two adjacent structures under a white-noise ground excitation. The fluid damper of the optimum parameters determined based on the white-noise ground excitation is then applied to link the adjacent structures subjected to either a filtered white-noise ground excitation or the El Centro 1940 NS ground excitation to examine the applicability of the analytical formulas to practical problems.

2. Basic equations

Let us consider two adjacent structures modeled as two s.d.o.f. systems as shown in Fig. 1. One s.d.o.f. system is called the primary structure or the P-structure and the other is the auxiliary structure or the A-structure. The natural frequencies and the damping ratios of the P-structure and the A-structure are ω_P, ω_A and ξ_P, ξ_A, respectively. Both structures are subjected to the same base acceleration. The effects due to spatial variations of the ground motion or due to soil–structure interactions are neglected. The studies carried out by Constantinou and Symans [8] show that the fluid damper applicable to civil structures can be described by the first order Maxwell model proposed by Bird et al. [11]:

$$f_I(t) + \lambda \frac{\mathrm{d}f_I(t)}{\mathrm{d}t} = C_0 \dot{x}(t), \tag{1a}$$

$$\dot{x}(t) = \dot{X}_A(t) - \dot{X}_P(t), \tag{1b}$$

where $f_I(t)$ is the damper force, λ is the relaxation time, C_0 is the damping coefficient at zero frequency, $\dot{x}(t)$ is the damper velocity, and $\dot{X}_P(t)$ and $\dot{X}_A(t)$ are the horizontal relative velocities of the P- and A-structures, respectively, with respect to the ground. The relaxation time λ can be approximately equal to C_0/k, that is, the ratio of the damping coefficient at zero frequency C_0 to the spring stiffness coefficient k of the damper system, in which one spring and one dashpot are connected in series (see Fig. 1).

The equations of motion of the structure–damper system can be written as

$$M_P \ddot{X}_P(t) + C_P \dot{X}_P(t) + K_P X_P(t) - f_I(t) = -M_P \ddot{X}_g(t), \tag{2a}$$

$$M_A \ddot{X}_A(t) + C_A \dot{X}_A(t) + K_A X_A(t) + f_I(t) = -M_A \ddot{X}_g(t), \tag{2b}$$

where M_P, K_P and C_P denote the mass, stiffness and damping coefficient of the P-structure, respectively; $X_P(t)$ is the horizontal relative displacement of the P-structure with respect to the ground; M_A, K_A and C_A denote the mass, stiffness and damping coefficient of the A-structure, respectively; $X_A(t)$ is the horizontal relative displacement of the A-structure with respect to the ground; and $\ddot{X}_g(t)$ is the horizontal ground acceleration, which is assumed as a white-noise random process with a constant spectral density of S_{gg}.

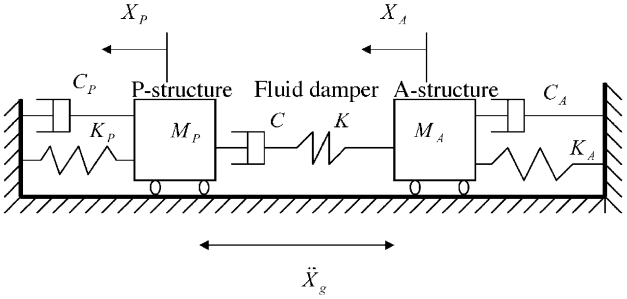

Fig. 1. Structural model of two adjacent structures linked by fluid damper.

The displacement responses of the P-structure and the A-structure in the frequency domain can be obtained from Eqs. (1) and (2) as

$$X_P(\mathrm{j}\omega) = \frac{\alpha_P(\mathrm{j}\omega)}{D(\mathrm{j}\omega)}\ddot{X}_g(\mathrm{j}\omega), \quad X_A(\mathrm{j}\omega) = \frac{\alpha_A(\mathrm{j}\omega)}{D(\mathrm{j}\omega)}\ddot{X}_g(\mathrm{j}\omega), \tag{3a, b}$$

where

$$D(\mathrm{j}\omega) = a_6(\mathrm{j}\omega)^6 + a_5(\mathrm{j}\omega)^5 + a_4(\mathrm{j}\omega)^4 + a_3(\mathrm{j}\omega)^3 + a_2(\mathrm{j}\omega)^2 + a_1(\mathrm{j}\omega) + a_0,$$

$$\alpha_P(\mathrm{j}\omega) = -[(1-(\mathrm{j}\omega\lambda)^2)(\omega_A^2 + 2\xi_A\omega_A(\mathrm{j}\omega) + (\mathrm{j}\omega)^2 + (1+\mu)\Delta_0(\mathrm{j}\omega - (\mathrm{j}\omega)^2\lambda))],$$

$$\alpha_A(\mathrm{j}\omega) = -[(1-(\mathrm{j}\omega\lambda)^2)(\omega_P^2 + 2\xi_P\omega_P(\mathrm{j}\omega) + (\mathrm{j}\omega)^2 + (1+\mu)\Delta_0(\mathrm{j}\omega - (\mathrm{j}\omega)^2\lambda))], \tag{4}$$

in which

$$a_0 = \omega_P^2\omega_A^2, \quad a_1 = 2\xi_P\omega_A^2\omega_P + 2\xi_A\omega_P^2\omega_A + \omega_A^2\Delta_0 + \omega_P^2\mu\Delta_0,$$

$$a_2 = \omega_A^2 + \omega_P^2 + 4\xi_P\xi_A\omega_P\omega_A + 2\xi_A\omega_A\Delta_0 + 2\xi_P\omega_P\mu\Delta_0 - \lambda\Delta_0\omega_A^2 - \mu\lambda\Delta_0\omega_P^2 - \lambda^2\omega_A^2\omega_P^2,$$

$$a_3 = 2\xi_A\omega_A + 2\xi_P\omega_P + (1+\mu)\Delta_0 - 2\lambda\Delta_0\xi_A\omega_A - 2\mu\lambda\Delta_0\xi_{PA}\omega_P - 2\lambda^2\xi_P\omega_P\omega_A^2 - 2\lambda^2\xi_A\omega_P^2\omega_A,$$

$$a_4 = 1 - \lambda\Delta_0(1+\mu) - \lambda^2(\omega_P^2 + \omega_A^2 + 4\xi_P\xi_A\omega_P\omega_A),$$

$$a_5 = -2\lambda^2(\xi_P\omega_P + \xi_A\omega_A), \quad a_6 = -\lambda^2, \quad \mu = \frac{M_P}{M_A}, \quad \Delta_0 = \frac{C_0}{M_P} \quad \text{and j = imaginary unit.} \tag{5}$$

It can be shown that the time-averaged total relative energy of the P-structure under the white-noise ground excitation is [12]

$$\bar{E}_P = \tfrac{1}{2}M_P\langle\dot{X}_P^2(t)\rangle + \tfrac{1}{2}K_P\langle X_P^2(t)\rangle = M_P\langle\dot{X}_P^2(t)\rangle = \frac{1}{2\pi}M_P\int_{-\infty}^{\infty} S_{\dot{X}_P\dot{X}_P}(\mathrm{j}\omega)\,\mathrm{d}\omega, \tag{6}$$

where $S_{\dot{X}_P\dot{X}_P}(\mathrm{j}\omega)$ is the power spectral density of the velocity response of the P-structure.

In consideration of Eq. (3) and $\dot{X}_P(\mathrm{j}\omega) = \mathrm{j}\omega X_P(\mathrm{j}\omega)$, the time-averaged energy of the P-structure can be obtained as [13]

$$\bar{E}_P = \frac{M_P S_{gg}}{2\pi\mathrm{j}}\int_{-\infty}^{\infty}\frac{(\mathrm{j}\omega\alpha_P(\mathrm{j}\omega))(\mathrm{j}\omega\alpha_P(\mathrm{j}\omega))^*}{D(\mathrm{j}\omega)D^*(\mathrm{j}\omega)}\,\mathrm{d}(\mathrm{j}\omega) = \frac{W_P M_P S_{gg}}{2a_6\Delta}, \tag{7}$$

where

$$(\mathrm{j}\omega\alpha_P(\mathrm{j}\omega))(\mathrm{j}\omega\alpha_P(\mathrm{j}\omega))^* = b_0(\mathrm{j}\omega)^{10} + b_1(\mathrm{j}\omega)^8 + b_2(\mathrm{j}\omega)^6 + b_3(\mathrm{j}\omega)^4 + b_4(\mathrm{j}\omega)^2 + b_5,$$

$$\begin{aligned}\Delta = {} & a_6^2a_1^3 + 3a_6a_5a_3a_1a_0 - 2a_6a_5a_2a_1^2 - a_6a_4a_3a_1^2 - a_6a_3^3a_0 + a_6a_3^2a_2a_1 + a_5^3a_0^2 - 2a_5^2a_4a_1a_0 \\ & - a_5^2a_3a_2a_0 + a_5^2a_2^2a_1 + a_5a_4^2a_1^2 + a_5a_4a_3^2a_0 - a_5a_4a_3a_2a_1,\end{aligned}$$

$$W_P = b_0\lambda_0 + a_6b_1\lambda_1 + a_6b_2\lambda_2 + a_6b_3\lambda_3 + a_6b_4\lambda_4 + (a_6b_5/a_0)\lambda_5, \tag{8}$$

in which

$$b_0 = -\lambda^4, \quad b_1 = 2\lambda^2 - 2\Delta_0\lambda^3 - 2\lambda^4\omega_A^2 + 4\lambda^4\xi_A^2\omega_A^2 - 2\mu\Delta_0\lambda^3,$$

$$b_2 = -1 + 2\lambda\Delta_0 + 4\lambda^2\omega_A^2 - 8\lambda^2\xi_A^2\omega_A^2 - 4\lambda^2\Delta_0\xi_A\omega_A - \lambda^2\Delta_0^2 - 2\lambda^3\Delta_0\omega_A^2 - (\lambda\omega_A)^4 + 2\mu\Delta\lambda_0 - 4\mu\lambda^2\Delta_0\xi_A\omega_A - 2\mu\lambda^2\Delta_0^2 - 2\mu\lambda^3\omega_A^2\Delta_0 - \mu^2\lambda^2\Delta_0^2,$$

$$b_3 = -2\omega_A^2 + 4\xi_A^2\omega_A^2 + 4\xi_A\omega_A\Delta_0 + \Delta_0^2 + 2\lambda\Delta_0\omega_A^2 + 2\lambda^2\omega_A^4 + 4\mu\xi_A\omega_A\Delta_0 + 2\mu\Delta_0^2 + 2\mu\lambda\omega_A^2\Delta_0 + \mu^2\Delta_0^2,$$

$$b_4 = -\omega_A^4, \quad b_5 = 0,$$

$$\lambda_0 = -a_6a_3a_1a_0 + a_6a_2a_1^2 - a_5^2a_0^2 + 2a_5a_4a_1a_0 + a_5a_3a_2a_0 - a_5a_2^2a_1 - a_4^2a_1^2 - a_4a_3^2a_0 + a_4a_3a_2a_1,$$

$$\lambda_1 = -a_5a_1a_0 + a_4a_1^2 + a_3^2a_0 - a_3a_2a_1, \quad \lambda_2 = -a_6a_1^2 - a_5a_3a_0 + a_5a_2a_1,$$

$$\lambda_3 = a_6a_3a_1 + a_5^2a_0 - a_5a_4a_1, \quad \lambda_4 = a_6a_5a_1 - a_6a_3^2 - a_5^2a_2 + a_5a_4a_3,$$

$$\lambda_5 = a_6^2a_1^2 + a_6a_5a_3a_0 - 2a_6a_5a_2a_1 - a_6a_4a_3a_1 + a_6a_3^2a_2 - a_5^2a_4a_0 + a_5^2a_2^2 + a_5a_4^2a_1 - a_5a_4a_3a_2,$$

In a similar way, the time-averaged energy of the A-structure can be obtained as

$$\bar{E}_A = \frac{M_A S_{gg}}{2\pi\mathrm{j}} \int_{-\infty}^{\infty} \frac{(\mathrm{j}\omega\alpha_A(\mathrm{j}\omega))(\mathrm{j}\omega\alpha_A(\mathrm{j}\omega))^*}{D(\mathrm{j}\omega)D^*(\mathrm{j}\omega)}\,\mathrm{d}(\mathrm{j}\omega) = \frac{W_A M_A S_{gg}}{2a_6\Delta}, \tag{9}$$

where

$$W_A = d_0\lambda_0 + a_6d_1\lambda_1 + a_6d_2\lambda_2 + a_6d_3\lambda_3 + a_6d_4\lambda_4 + (a_6d_5/a_0)\lambda_5, \tag{10}$$

in which

$$d_0 = -\lambda^4, \quad d_1 = 2\lambda^2 - 2\Delta_0\lambda^3 - 2\lambda^4\omega_P^2 + 4\lambda^4\xi_P^2\omega_P^2 - 2\mu\Delta_0\lambda^3,$$

$$d_2 = -1 + 2\lambda\Delta_0 + 4\lambda^2\omega_P^2 - 8\lambda^2\xi_P^2\omega_P^2 - 4\lambda^2\Delta_0\xi_P\omega_P - \lambda^2\Delta_0^2 - 2\lambda^3\Delta_0\omega_P^2 - (\lambda\omega_P)^4 + 2\mu\Delta\lambda_0 - 4\mu\lambda^2\Delta_0\xi_P\omega_P - 2\mu\lambda^2\Delta_0^2 - 2\mu\lambda^3\omega_P^2\Delta_0 - \mu^2\lambda^2\Delta_0^2,$$

$$d_3 = -2\omega_P^2 + 4\xi_P^2\omega_P^2 + 4\xi_P\omega_P\Delta_0 + \Delta_0^2 + 2\lambda\Delta_0\omega_P^2 + 2\lambda^2\omega_P^4 + 4\mu\xi_P\omega_P\Delta_0 + 2\mu\Delta_0^2 + 2\mu\lambda\omega_P^2\Delta_0 + \mu^2\Delta_0^2,$$

$$d_4 = -\omega_P^4, \quad d_5 = 0.$$

The total time-averaged energy of the two adjacent structures linked by a fluid damper subjected to the white-noise ground excitation can be obtained by adding Eqs. (7) and (9) together, that is,

$$\bar{E} = \bar{E}_P + \bar{E}_A = \frac{(W_P M_P + W_A M_A)S_{gg}}{2a_6\Delta}. \tag{11}$$

3. Formulas for optimum parameters

The structural optimization criteria depend on the dynamic forces acting on the structure and the structural response quantities of interest. Minimizing the story drift or the absolute

acceleration of a controlled structure subjected to a ground motion has been considered as an optimization objective [5]. The study of Hayen and Iwan [14] further shows that it is the relative vibration energy of the structure to the ground that provides an upper bound for the absolute value of the story drift. Thus, the relative vibration energy of the structure is selected as the structural response quantity of interest in this study. Furthermore, to derive the explicit formulas for the optimum parameters of the fluid damper as the function of the main structure parameters, the white-noise ground motion is assumed.

3.1. The first optimization criterion

The first optimization criterion is to minimize the relative vibration energy of the primary structure (the P-structure) only. Correspondingly, the following two conditions should be satisfied:

$$\frac{\partial \bar{E}_P}{\partial \xi} = 0, \quad \frac{\partial \bar{E}_P}{\partial \chi} = 0, \tag{12}$$

where $\xi = C_0/2M_P\omega_P$ and $\chi = \lambda\omega_P$ are the damping ratio at zero frequency and the non-dimensional relaxation time, respectively.

Since the structural damping ratio in the original adjacent structures is small compared with that generated by the fluid damper, the structural damping of the adjacent structures is assumed to be zero in the derivation of the formulas. This simplification ensures that the formulas can be explicitly expressed as functions of the mass and frequency ratios of the two structures only. This simplification also implies that the structural damping has no significant effect on the optimum parameters of the fluid damper. The rationality and two expectations of this simplification will be examined in the numerical examples in which the structural damping ratios of adjacent structures will be included. As a result, substituting $\xi_P = \xi_A = 0$ into Eq. (7) and then solving Eq. (12) give the optimum parameters of the Maxwell model-defined damper linking two adjacent structures as

(1) when $\beta < 1$:

$$\xi_{opt} = \frac{(1-\beta^2)\sqrt{\mu}}{\sqrt{-\mu\beta^4 + \mu(3+4\mu) + (4+6\mu)\beta^2}},$$

$$\chi_{opt} = \frac{(1+2\mu+\beta^2)\sqrt{\mu}}{\sqrt{-\mu\beta^4 + \mu(3+4\mu) + (4+6\mu)\beta^2}}, \tag{13a, b}$$

(2) when $\beta = 1$:

$$\xi_{opt} = 0, \quad \chi_{opt} = 0, \tag{13c, d}$$

(3) when $\beta > 1$:

$$\xi_{opt} = \frac{(\beta^2-1)\sqrt{\mu}}{2(1+\mu)\sqrt{\mu+\beta^2}}, \quad \chi_{opt} = 0, \tag{13e, f}$$

where $\beta = \omega_A/\omega_P$.

It is seen from Eqs. (13c,d) that when the natural frequency of the P-structure is equal to the A-structure, the optimum damping ratio and relaxation time of the damper are zero, which indicates that the fluid damper does not function at all. Another special case is that the natural frequency of the A-structure is equal to zero, that is, the A-structure becomes only a mass block connected to the P-structure through a fluid damper. The optimum parameters of the fluid damper used for this special case, where the frequency ratio β is equal to zero, can be found from Eqs. (13a,b) as

$$\xi_{opt\text{-}TMD} = \frac{1}{\sqrt{3+4\mu}}, \quad \chi_{opt\text{-}TMD} = \frac{1+2\mu}{\sqrt{3+4\mu}}. \tag{14a, b}$$

Clearly, these formulas are different from those for a tuned mass damper connected to a building through a spring and a viscous damper arranged in parallel [9]. The general understanding of Eq. (13) based on the first optimization criterion for the optimum parameters of the fluid damper linking the adjacent structures is given as follows.

First of all, Eq. (13) demonstrates that the optimal parameters ξ and χ depend on the mass and frequency ratios of the two adjacent structures only. The variations of the optimum parameters ξ and χ of the fluid damper with the mass and frequency ratios of the two structures are plotted in Fig. 2. Only the value χ when $\beta<1$ is shown in Fig. 2b because the optimum value χ is equal to zero when $\beta\geqslant 1$. It is seen that when the natural frequency of the A-structure is larger than that of the P-structure (i.e., $\beta > 1$), the optimum damping ratio increases with increasing frequency ratio β while the optimum relaxation time is equal to zero. This implies that when the A-structure is stiffer than the P-structure, the stiffness of the fluid damper should be infinitely large and the fluid damper actually becomes a viscous damper that dissipates the vibration energy of the P-structure. When the natural frequency of the A-structure is smaller than that of the P-structure (i.e., $\beta<1$), the optimum damping ratio increases moderately with decreasing frequency ratio β while the optimum relaxation time remains almost unchanged with the frequency ratio. It can also be observed from Fig. 2 that the optimum damping ratio and relaxation time of the damper depend on the mass ratio μ of the two structures. The optimum damping ratio achieves its maximum value when $\mu = 1$ for a given frequency ratio, and it decreases as μ is away from unit. The optimum relaxation time, however, always increases as μ increases, which implies that the smaller is the mass of the A-structure, the less the stiffness of the damper.

To examine the control effectiveness of the fluid damper, the root mean square (r.m.s.) values of relative displacement response of the P-structure and the A-structure linked by the fluid damper of optimum parameters ξ and χ under the white-noise ground motion are compared with those of the two adjacent structures subjected to the same ground motion but without control. The control effectiveness indexes are accordingly defined as

$$R_P = \frac{\langle X_P \rangle_{Controlled}}{\langle X_P \rangle_{Uncontrolled}}, \quad R_A = \frac{\langle X_A \rangle_{Controlled}}{\langle X_A \rangle_{Uncontrolled}}, \tag{15}$$

where $\langle X_P \rangle_{Controlled}$ and $\langle X_A \rangle_{Controlled}$ denote the r.m.s. values of relative displacement response of the P-structure and the A-structure, respectively, linked by the fluid damper of optimum parameters and under the white-noise ground motion. $\langle X_P \rangle_{Uncontrolled}$ and $\langle X_A \rangle_{Uncontrolled}$ denote the r.m.s. values of relative displacement response of the P-structure and the A-structure, respectively, subjected to the same ground motion but without any control. In the computation of

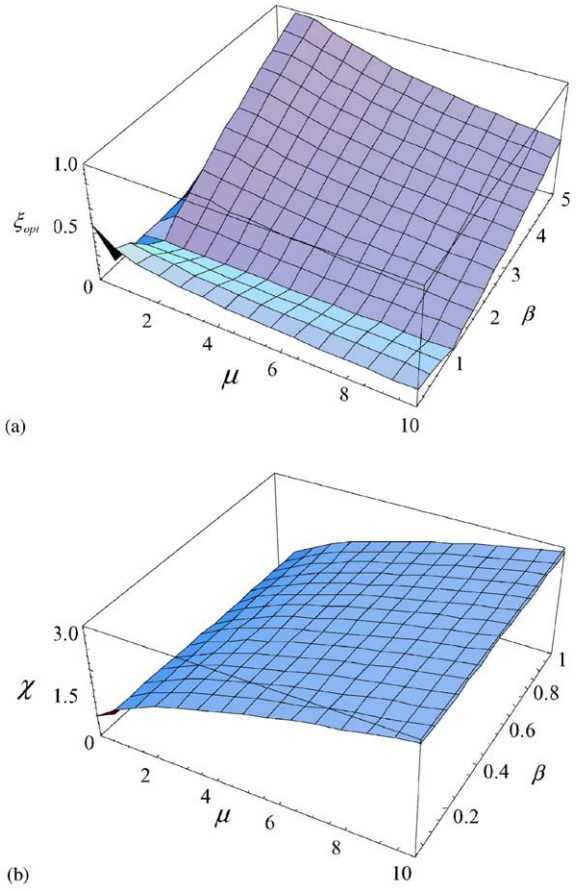

Fig. 2. Variations of optimum parameters with mass and frequency ratios (Criterion 1): (a) the optimum damping coefficient at zero frequency ξ, (b) the optimum relaxation time χ.

the effectiveness indexes, the structural damping ratios ξ_P and ξ_A of the two structures are included and taken as 0.02 to confirm the rationality and two expectations of the simplification used in the derivation of formulas for the optimum parameters of the damper and to consider real situation as well.

The variations of the control effectiveness indexes R_P and R_A with the mass ratio μ and the frequency ratio β are deployed in Fig. 3 in a three-dimensional form and in Fig. 4 in a two-dimensional form. It is seen that the optimal control effectiveness significantly depends on the frequency ratio β. When the frequency ratio β approaches unit, the damper has no effect on the P-structure and actually enlarges the response of the A-structure when the mass ratio is over 5. When the frequency ratio increases from unit or decreases from unit, the response of the P-structure becomes smaller and smaller. The control effectiveness also increases with decreasing mass ratio to certain level. For instance, at a frequency ratio of 2 and a mass ratio of 2, the response of the P-structure can be reduced by about 60%. For the A-structure, if the frequency ratio is larger than 1.5, its response is also reduced significantly although

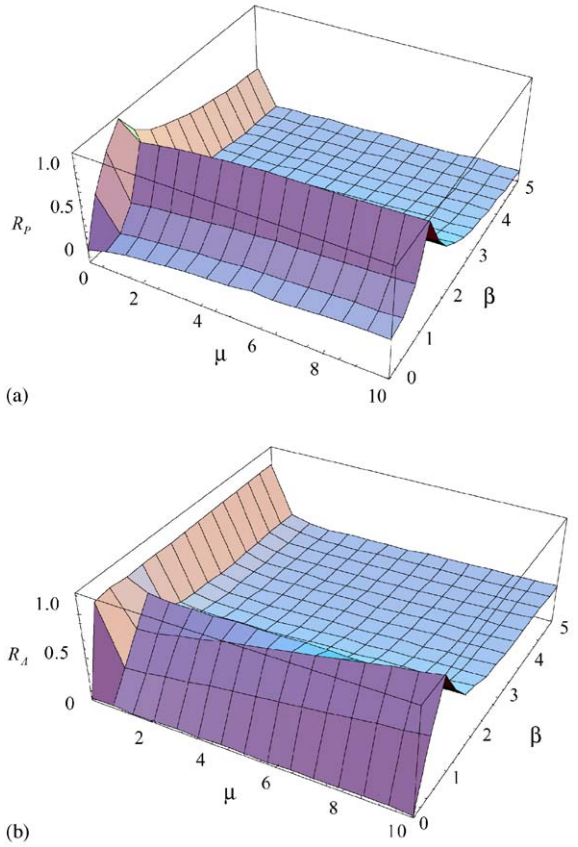

Fig. 3. Variations of control effectiveness indexes with mass and frequency ratios (Criterion 1): (a) P-structure, (b) A-structure.

the first optimization criterion does not considers the minimization of the A-structure response. However, if the frequency ratio is between 0.8 and 1.0 and the mass ratio is over 5, the response of the A-structure will be larger than that of the same structure without control. It is also seen from Figs. 4(c,d) that there is a optimum mass ratio, by which the response of the structure is the smallest. Furthermore, the optimum mass ratio is quite small and different for the two structures.

3.2. The second optimization criterion

The second optimization criterion is to minimize the total vibration energy of the two adjacent structures with the following two conditions being satisfied:

$$\frac{\partial \bar{E}}{\partial \xi} = 0, \quad \frac{\partial \bar{E}}{\partial \chi} = 0. \tag{16}$$

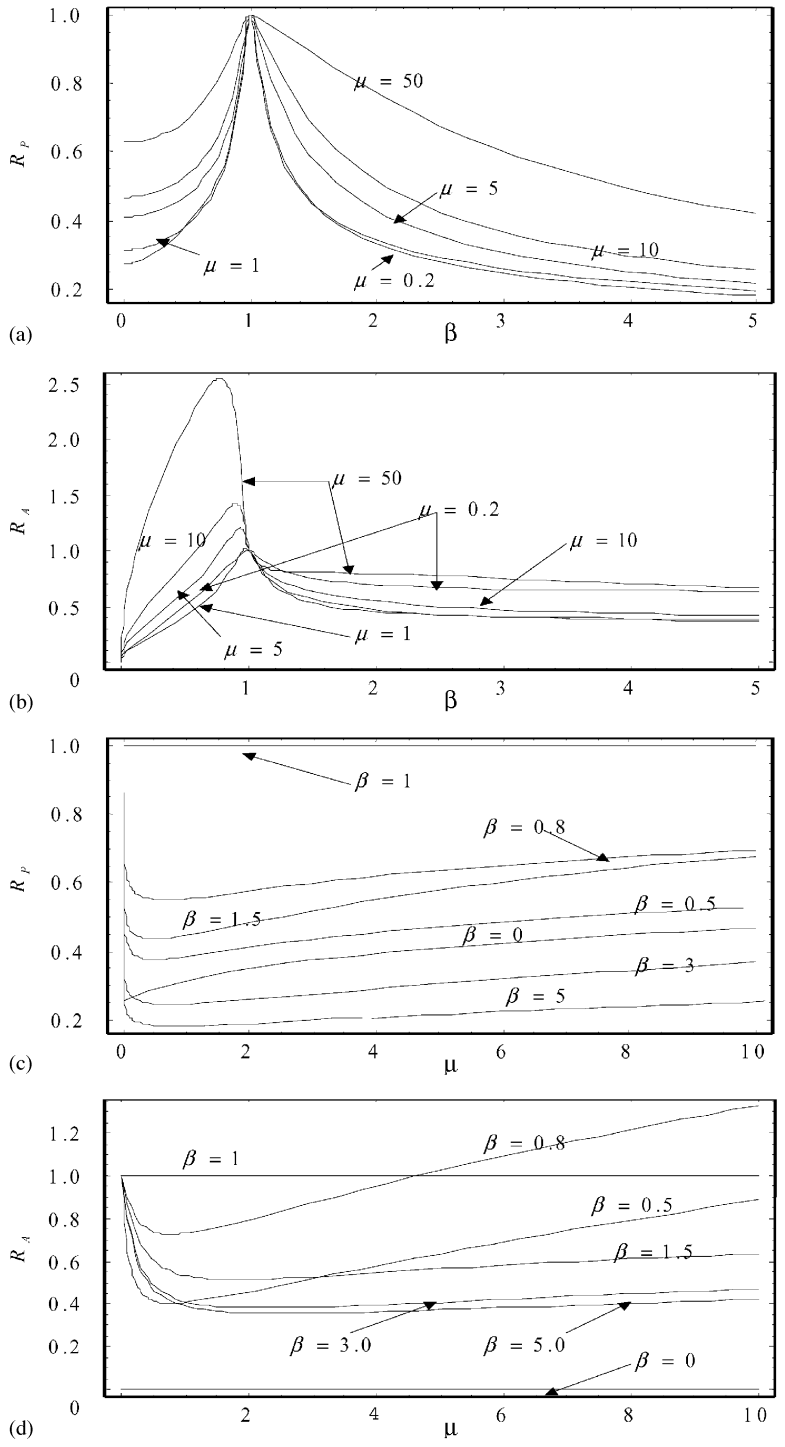

Fig. 4. Effects of mass and frequency ratios on control performance (Criterion 1): (a) R_P vs. β, (b) R_A vs. β, (c) R_P vs. μ, (d) R_A vs. μ.

Compared with the first optimization criterion that focuses on the vibration reduction of the P-structure only, the second criterion treats the two structures of the same importance. Thus, the name of which structure is P-structure or A-structure is not essential. To facilitate the following discussion, the frequency ratio is then restricted to $\beta \leqslant 1$, that is, the P-structure is stiffer than the A-structure. However, the obtained results are also applicable to the case of $\beta \succ 1$ only if the names of the two structures are swapped.

Again, the structural damping ratios of the two structures are assumed to be zero when deriving the optimization formulas based on the second criterion. By assuming the structural damping ratios $\xi_P = \xi_A = 0$ in Eq. (11) and then substituting Eq. (11) to Eq. (16), the optimum parameters of the fluid damper can be obtained as

(1) when $\mu \geqslant 1$:

$$\xi_{opt} = \frac{\sqrt{(1+\mu^2)(\mu^2+\beta^2)(1-\beta^2)^2}}{(1+\mu)\sqrt{\mu((8-\mu)\beta^4+\mu(8\mu-1)+18\mu\beta^2)}},$$

$$\chi_{opt} = \frac{((\mu-2)\beta^2+\mu(2\mu-1))\sqrt{1+\mu^2}}{\sqrt{\mu(\mu^2+\beta^2)((8-\mu)\beta^4+\mu(8\mu-1)+18\mu\beta^2)}}, \tag{17a, b}$$

(2) when $\mu < 1$ and $\beta^2 < \mu(2\mu-1)/(2-\mu)$:

$$\xi_{opt} = \frac{\sqrt{(1+\mu^2)(\mu^2+\beta^2)(1-\beta^2)^2}}{(1+\mu)\sqrt{\mu((8-\mu)\beta^4+\mu(8\mu-1)+18\mu\beta^2)}},$$

$$\chi_{opt} = \frac{((\mu-2)\beta^2+\mu(2\mu-1))\sqrt{1+\mu^2}}{\sqrt{\mu(\mu^2+\beta^2)((8-\mu)\beta^4+\mu(8\mu-1)+18\mu\beta^2)}}, \tag{17c, d}$$

(3) when $\mu < 1$ and $\beta^2 \geqslant \mu(2\mu-1)/(2-\mu)$:

$$\xi_{opt} = \frac{\sqrt{(1+\mu^2)(1-\beta^2)^2}}{2(1+\mu)\sqrt{(1+\mu)(\mu+\beta^2)}}, \quad \chi_{opt} = 0. \tag{17e, f}$$

Eq. (17) also shows that the optimum parameters ξ and χ of the fluid damper depend on the mass and frequency ratios of the two structures only. The variations of the optimum damping ratio at zero frequency ξ and the optimum relaxation time χ with the mass and frequency ratios of the two structures, μ and β, are shown in Fig. 5. It is seen that the value of the optimum parameter ξ decreases as the frequency ratio and the mass ratio increase. The value of the optimum parameter χ decreases with increasing frequency ratio but it increases with increasing mass ratio. The variations of control effectiveness indexes R_P and R_A with the mass and frequency ratios μ and β obtained from the second optimization criterion are shown in Fig. 6 in a three-dimensional form and in Fig. 7 in a two-dimensional form. It is seen that the response of the P-structure is always smaller than unit except when the mass of the P-structure is further less than the mass of

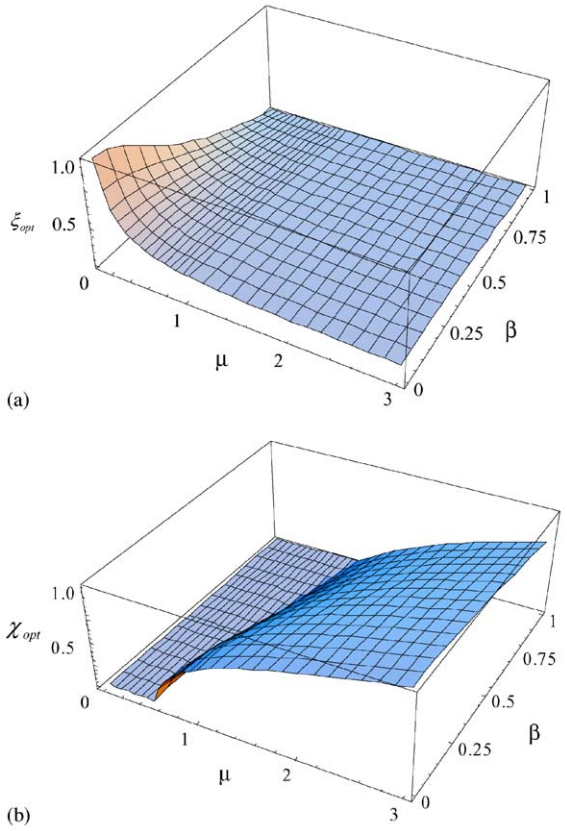

Fig. 5. Variations of optimum parameters with mass and frequency ratios (Criterion 2): (a) the optimum damping coefficient at zero frequency ξ, (b) the optimum relaxation time χ.

A-structure or the frequency ratio is equal to 1. The response of the P-structure decreases with decreasing frequency ratio and mass ratio when the mass ratio is greater than a value around 0.5. The response of the P-structure increases with decreasing mass ratio when the mass ratio is less than a value around 0.5. To be effective in reducing the response of the A-structure, the mass ratio of the two structures should not be too large and the frequency ratio should not approach the unit. In general the response of the A-structure decreases with decreasing frequency ratio and mass ratio if the mass ratio is greater than a value around 0.5.

In summary, the two optimization criteria proposed in this study can explicitly express the optimum parameters of the Maxwell model-defined fluid damper linking two adjacent structures as the function of the mass and frequency ratios of the two structures if the structural damping ratios of the structures are assumed to be zero and the ground motion is assumed to be a white noise excitation. The results show that with either the optimization criterion, the control effectiveness of the damper increases as the difference of the natural frequencies of the two structures increases. There is an optimum mass ratio, by which the response of the structure is minimized. However, when the natural frequencies of the two structures are very close to each other, the damper has no function at all.

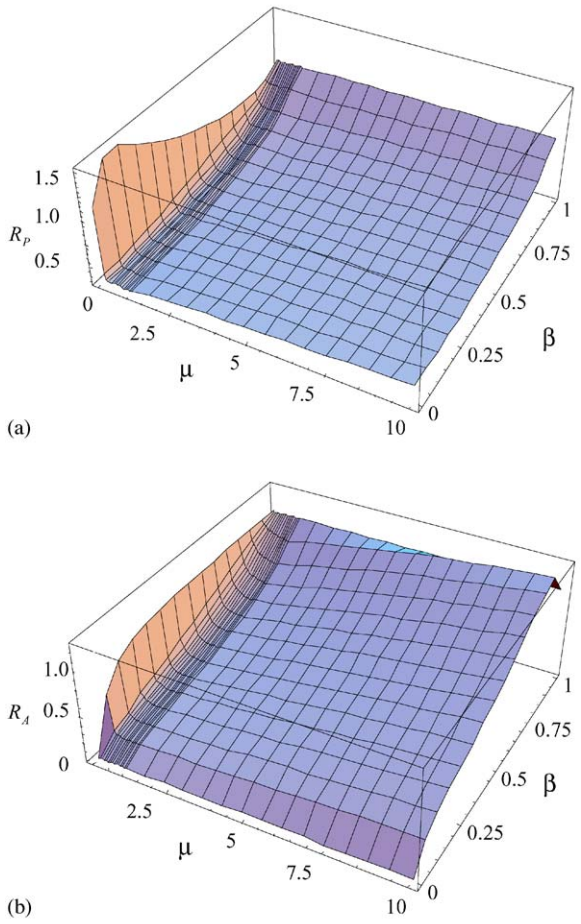

Fig. 6. Variations of control effectiveness indexes with mass and frequency ratios (Criterion 2): (a) P-structure, (b) A-structure.

4. Applications

The optimum parameters of the fluid damper derived above are based on the stationary white-noise ground motion. To examine their applicability to the adjacent structures subjected to either a filtered white-noise ground motion or a field-recorded seismic ground motion, three pairs of adjacent structures are selected as examples for application. The structural parameters of each pair of adjacent structures are listed below:

Example 1: $M_P = 2.58 \times 10^7$ kg, $\omega_P = 4.27$ rad/s, $\xi_P = 0.01$, $\mu = 1$, $\beta = 0.70726$, $\gamma = 1$,
Example 2: $M_P = 1.5 \times 10^5$ kg, $\omega_P = 10.55$ rad/s, $\xi_P = 0.02$, $\mu = 2$, $\beta = 0.5$, $\gamma = 2$,
Example 3: $M_P = 1.5 \times 10^5$ kg, $\omega_P = 10.55$ rad/s, $\xi_P = 0.02$, $\mu = 5/3$, $\beta = 1.428$, $\gamma = 1$.

The natural frequencies of the two adjacent structures in the first example are relatively close and small, representing the two tall buildings of similar dynamic properties. The second and

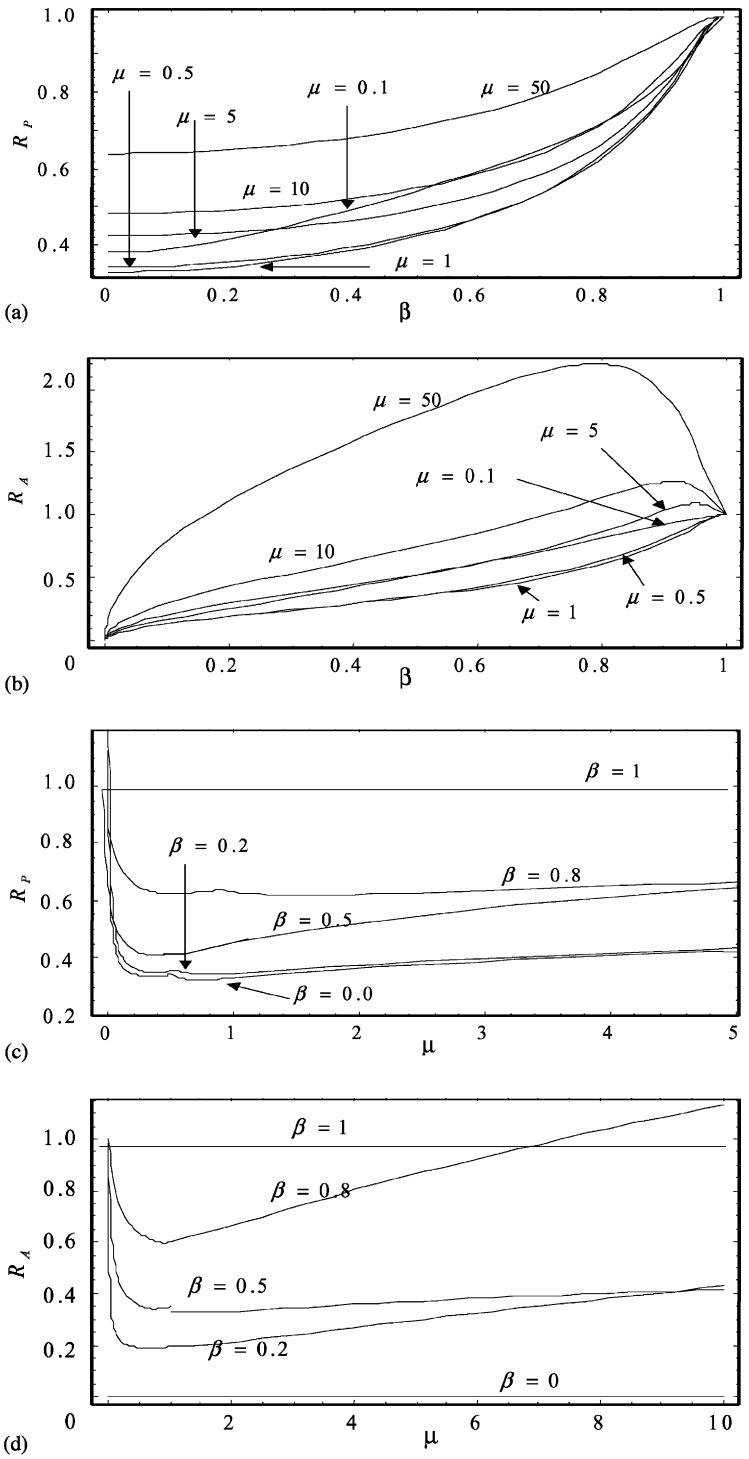

Fig. 7. Effects of mass and frequency ratios on control performance (Criterion 2): (a) R_P vs. β, (b) R_A vs. β, (c) R_P vs. μ, (d) R_A vs. μ.

third examples represent the two low-rise buildings, of which the natural frequencies depart from each other, but the A-structure in the second example is softer than the P-structure while the A-structure in the third example is stiffer than the P-structure.

4.1. Optimum parameters of damper

The optimum parameters of the fluid damper for each pair of the adjacent structures using the derived analytical formulas are first found for the case of the white-noise ground motion and without considering the structural damping ratios of two adjacent structures. Table 1 lists the non-dimensional optimum values of damping coefficient at zero frequency ξ and the relaxation time χ of the fluid damper for each pair of the adjacent structures, obtained from Eqs. (13) and (17), respectively, based on either the first optimization criterion or the second optimization criterion. Then, these optimum parameters are used to compute the control effectiveness indexes R_P and R_A for each pair of the adjacent structures based on Eq. (15), and the results are tabulated in Table 2. It is observed that the responses of the two adjacent structures can be reduced significantly after the Maxwell model-defined fluid damper of the optimum parameters is used to link the two structures no matter which the optimization criterion is used. In general, the first optimization criterion leads to slightly larger response reduction of the P-structure compared with the second optimization criterion. On the contrary, the second optimization criterion results in larger response reduction of the A-structure compared with the first optimization criterion.

4.2. Modal frequencies and damping ratios

To understand why the fluid damper of optimum parameters can effectively reduce the dynamic responses of the two structures in the above three examples, the natural frequencies and modal

Table 1
The optimum parameter values of the fluid damper in the three examples

	Non-dimensional damping coefficient at zero frequency ξ		Non-dimensional relaxation time χ	
	Criterion 1	Criterion 2	Criterion 1	Criterion 2
Example 1	0.146	0.103	1.021	0.137
Example 2	0.209	0.130	1.460	0.733
Example 3	0.131	0.120	0	0

Table 2
Control effectiveness indexes (stationary white-noise excitation)

	Criterion 1		Criterion 2	
	P-structure (R_P) (%)	A-structure (R_A) (%)	P-structure (R_P) (%)	A-structure (R_A) (%)
Example 1	35.3	45.8	40.1	36.8
Example 2	41.1	62.3	43.8	52.9
Example 3	50.1	53.7	50.3	53.4

Table 3
The comparison of natural frequencies and modal damping ratios of adjacent structures with and without the fluid damper

	Without damper		With damper (Criterion 1)		With damper (Criterion 2)	
	Frequency (rad/s)	Damping ratio (%)	Frequency (rad/s)	Damping ratio (%)	Frequency (rad/s)	Damping ratio (%)
Example 1	3.02	1	3.37	7.36	3.19	15.49
	4.27	1	4.66	11.55	4.08	12.20
Example 2	5.275	4	8.05	15.33	8.05	34.42
	10.55	2	12.26	13.86	10.72	21.29
Example 3	10.55	2	11.19	14.68	11.06	13.83
	15.07	2	13.82	18.41	14.04	16.89

damping ratios of the adjacent structures linked by the fluid damper are computed through a complex eigenvalue analysis, and the results are listed in Table 3 and compared with those of the adjacent structures without control. It is seen that with the installation of the fluid damper of optimum parameters, the damping ratios of the system are increased significantly. This is the main reason why the responses of both structures are reduced considerably. In addition, the change of the natural frequencies of the adjacent structures in Examples 1 and 3 are not over 10% compared with the adjacent structures without control. However, for the adjacent structures in Example 2, the change of the natural frequencies are over 40% because of the larger λ and ξ of the damper and the small frequency ratio.

4.3. Seismic response under filtered white-noise ground motion

The fluid damper of the optimum parameters determined based on the white-noise ground excitation is now applied to link the adjacent structures subjected to a filtered white-noise ground excitation to examine the applicability of the analytical formulas to practical problems. The Kanai–Tajimi filtered white-noise ground motion model, which has been widely used in earthquake engineering [15], can be represented by the following spectrum:

$$S(\omega) = S_0 \left[\frac{\omega_g^4 + 4\omega_g^2 \varsigma_g^2 \omega^2}{(\omega^2 - \omega_g^2)^2 + 4\omega_g^2 \varsigma_g^2 \omega^2} \right], \tag{18}$$

where ς_g, ω_g and S_0 are the characteristic parameters of the soil surrounding the adjacent structures. Three groups of the characteristic parameters, which represent firm, mid-firm and soft soil, respectively [16], are used in this study:

Group I: $\varsigma_g = 0.60$, $\omega_g = 15.60$ rad/s, $S_0 = 4.8 \times 10^{-3}$ m^2/s^3,
Group II: $\varsigma_g = 0.50$, $\omega_g = 10.55$ rad/s, $S_0 = 4.8 \times 10^{-3}$ m^2/s^3,
Group III: $\varsigma_g = 0.30$, $\omega_g = 3.14$ rad/s, $S_0 = 4.8 \times 10^{-3}$ m^2/s^3,

The intensity of ground motion $S_0 = 4.8 \times 10^{-3}$ m^2/s^3 is chosen to represent the intensity of the NS component of the 1940 El Centro earthquake [17]. Table 4 lists the r.m.s. relative displacement

Table 4
The root mean square relative displacement responses of P-structure and A-structure under filtered white-noise excitation

Earthquake excitation	Example	P-structure (cm)			A-structure (cm)		
		Non-control	Criterion 1	Criterion 2	Non-control	Criterion 1	Criterion 2
I	1	10.55	4.00	4.52	17.15	7.13	5.81
	2	2.35	0.99	1.05	3.96	1.84	1.63
	3	2.35	1.08	1.09	1.37	0.83	0.82
II	1	11.42	4.27	4.83	17.89	7.50	6.10
	2	2.51	1.08	1.14	4.42	2.08	1.82
	3	2.51	1.09	1.10	0.77	0.77	0.75
III	1	10.92	5.72	6.16	32.40	11.62	9.29
	2	0.50	0.44	0.43	2.86	1.10	1.23
	3	0.50	0.35	0.36	0.21	0.19	0.18

responses of the two structures to the ground before and after control under the filtered white-noise ground motions selected. It is seen that in most cases, the use of the fluid damper of the optimum parameters determined based on the white-noise ground motion can reduce the responses of both structures more than 50%. Except for the adjacent structures in Example 2 under the excitation II, the response of the P-structure determined using the first optimization criterion is slightly smaller than that determined using the second optimization criterion. On the other hand, except for the adjacent structures in Example 2 under the excitation III, the response of the A-structure determined using the second optimization criterion is smaller than that determined using the first optimization criterion. These results are very similar to those in the case of the white-noise ground motion, indicating the applicability of the analytical formulas for optimum parameters derived based on the white-noise ground motion. However, it should be noticed that there are some cases in which the response reduction of either the P-structure or the A-structure is very small. This is because either the dominant excitation frequency is far away from the natural frequency of the structure (e.g., Example 3 under the excitation III) or the installation of the fluid damper makes the frequency of the structure more close to the dominant excitation frequency (e.g., Example 3 under the excitation II).

4.4. Seismic response under El Centro 1940 NS excitation

The fluid damper of the optimum parameters determined based on the white-noise ground excitation is now applied to link the adjacent structures subjected to the El Centro 1940 NS earthquake to examine the applicability of the analytical formulas to practical problems. The peak acceleration of the El Centro 1940 NS earthquake is scaled to $0.14g$. The dynamic analysis of the adjacent structures linked by the Maxwell model-defined fluid damper in the time domain can be performed by merging Eq. (1) with Eq. (2) and by assuming that $\dot{f}_T(t)$ is constant within a time

interval [18]:

$$f_I(t_n) = f_I(t_{n-1}) + \frac{\Delta t}{2}(\dot{f}_I(t_n) + \dot{f}_I(t_{n-1})), \tag{19}$$

where Δt is the time interval between t_n and t_{n-1}. Eq. (1) can be then expressed as

$$f_I(t_n) = \frac{C_0 \Delta t}{2\lambda + \Delta t}(\dot{x}(t_n) + \dot{x}(t_{n-1})) + \frac{2\lambda - \Delta t}{2\lambda + \Delta t} f_I(t_{n-1}). \tag{20}$$

The substitution of Eq. (20) into Eq. (2) yields the system equation in a discrete time form as

$$M_P \ddot{X}_P(t_n) + C_P \dot{X}_P(t_n) + K_P X_P(t_n) - \frac{C_0 \Delta t}{2\lambda + \Delta t}(\dot{x}(t_n) + \dot{x}(t_{n-1})) - \frac{2\lambda - \Delta t}{2\lambda + \Delta t} f_I(t_{n-1}) = -M_P \ddot{X}_g(t_n), \tag{21a}$$

$$M_A \ddot{X}_A(t_n) + C_A \dot{X}_A(t_n) + K_A X_A(t_n) + \frac{C_0 \Delta t}{2\lambda + \Delta t}(\dot{x}(t_n) + \dot{x}(t_{n-1})) + \frac{2\lambda - \Delta t}{2\lambda + \Delta t} f_I(t_{n-1}) = -M_A \ddot{X}_g(t_n). \tag{21b}$$

Eq. (21) can be solved using the conventional numerical integration scheme. In this study the Wilson θ method is adopted.

The peak and r.m.s. relative displacement and absolute acceleration responses of the two structures in the three examples are computed and listed in Table 5 and compared with those of the structures without control. It is observed that the fluid damper of the optimum parameters determined based on the white-noise ground motion can also reduce the responses of both the structures under the real earthquake excitation. In most cases, the responses of both the structures are reduced by more than 30%, moderately smaller than that in the case of either the white-noise ground excitation or the filtered white-noise ground excitation. In general, the peak response reduction is less than the r.m.s. response reduction. Fig. 8 displays the time histories of the relative displacement response and the absolute acceleration response of the two structures in Example 2 using the first optimization criterion while Fig. 9 shows the time histories of the same quantities but using the second optimization criterion. The time histories of the same quantities of the two

Table 5
Peak and root mean square responses of the adjacent structures linked by optimized fluid damper subjected to El Centro 1940 NS earthquake excitation

			Example 1			Example 2			Example 3		
			Uncontrol	Criterion 1	Criterion 2	Uncontrol	Criterion 1	Criterion 2	Uncontrol	Criterion 1	Criterion 2
P	Peak	Dis. (cm)	16.16	11.17	12.17	3.04	2.28	2.30	3.04	1.70	1.73
		Acc.(gal)	294.59	216.73	206.02	339.41	227.32	225.20	339.41	226.34	229.04
	RMS	Dis.(cm)	5.14	3.51	3.70	0.90	0.50	0.49	0.90	0.39	0.39
		Acc.(gal)	93.69	55.61	57.98	100.60	46.21	46.18	100.60	47.38	48.04
A	Peak	Dis.(cm)	30.39	20.06	16.48	12.99	3.93	4.57	1.56	1.16	1.18
		Acc.(gal)	277.24	234.92	188.34	362.83	262.41	224.44	355.10	223.01	225.89
	RMS	Dis.(cm)	10.20	6.42	4.61	3.18	1.07	1.00	0.42	0.24	0.24
		Acc.(gal)	93.02	74.48	52.47	88.84	62.36	51.09	96.20	45.36	45.74

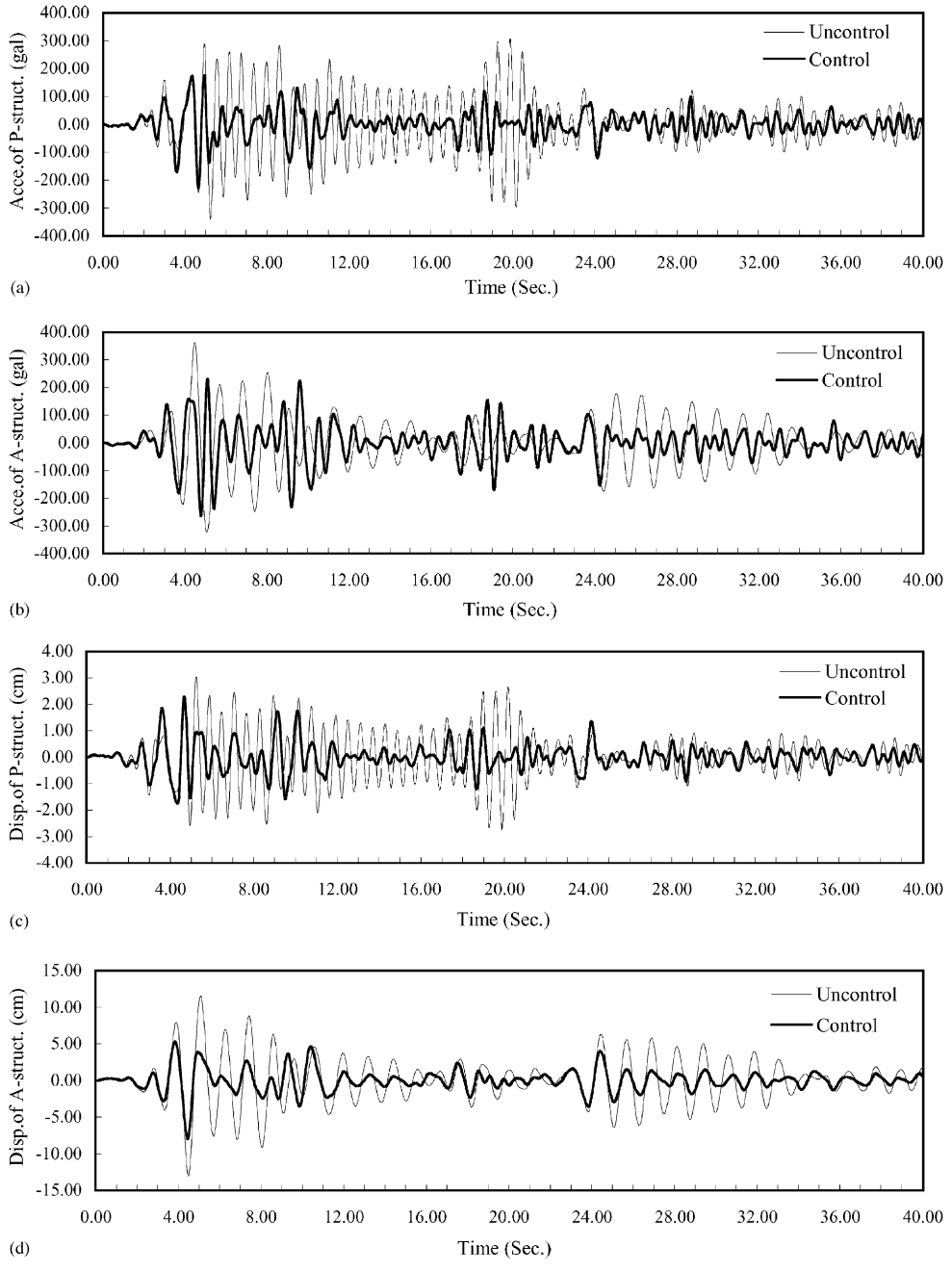

Fig. 8. Time histories of absolute acceleration and relative displacement response of the two structures under El Centro 1940 NS excitation (Example 2 and Criterion 1): (a) acceleration response of P-structure, (b) acceleration response of A-structure, (c) relative displacement response of P-structure, (d) relative displacement response of A-structure.

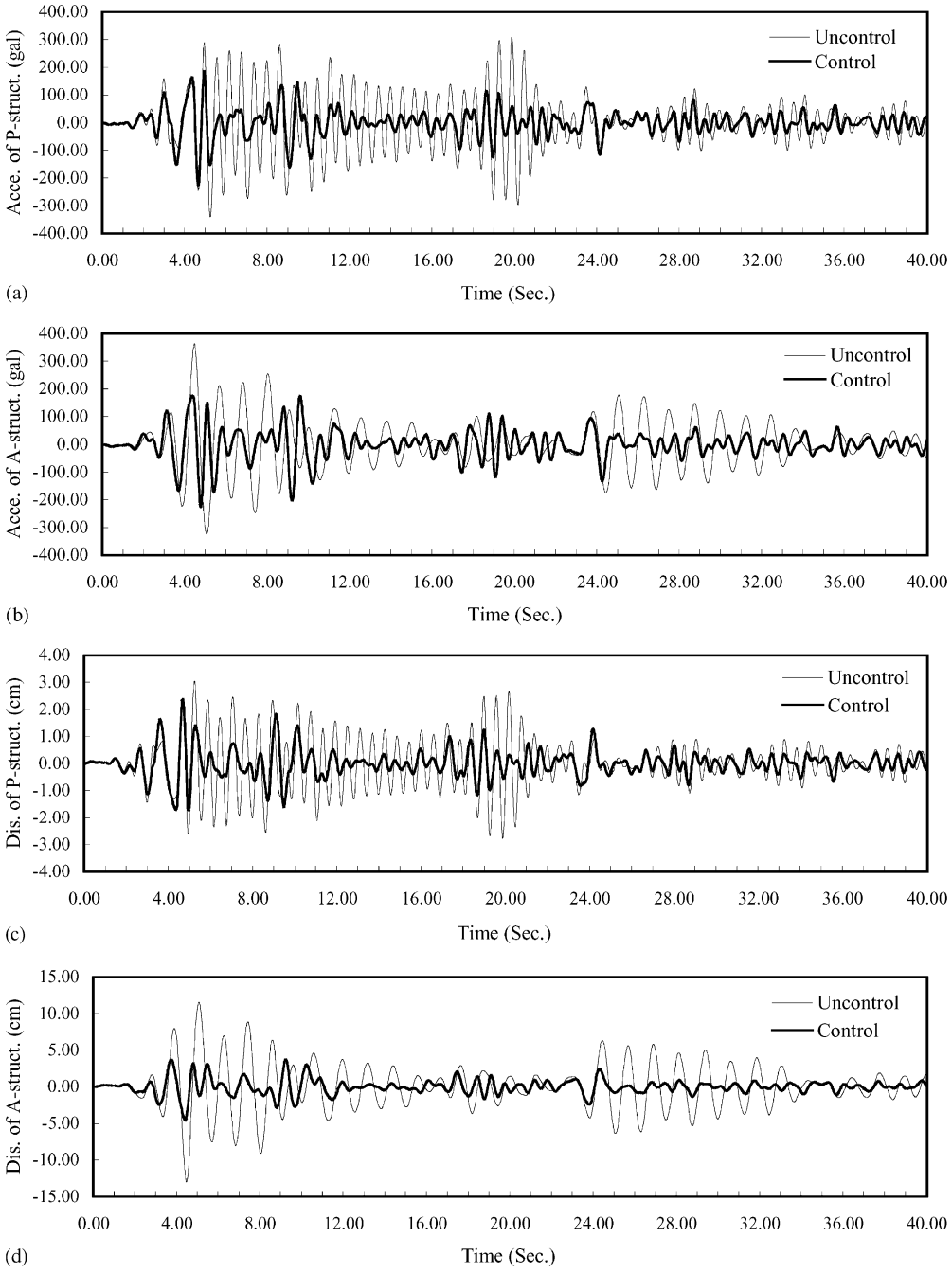

Fig. 9. Time histories of absolute acceleration and relative displacement response of the two structures under El Centro 1940 NS excitation (Example 2 and Criterion 2): (a) acceleration response of P-structure, (b) acceleration response of A-structure, (c) relative displacement response of P-structure, (d) relative displacement response of A-structure.

structures without control are also plotted in these two figures for comparison. The significant reductions of the relative displacement response and the absolute acceleration response of the two structures can be observed from the two figures, which demonstrate that the use of the fluid damper of optimum parameters to link the two adjacent structures is beneficial to reduce the seismic responses of both the structures and to prevent from the problem of pounding between the two structures. For the limit of space, the time-histories of the relative displacements and absolute accelerations of both the adjacent structures in Examples 1 and 3 under the two criteria for the uncontrolled and controlled systems are not given here.

5. Conclusions

The two optimization criteria have been proposed and the analytical formulas have been derived for determining optimum parameters of Maxwell model-defined fluid dampers used to link two adjacent structures under a white-noise ground excitation. The optimum parameters of the fluid damper can be explicitly expressed as the functions of the frequency and mass ratios of two adjacent structures if the structural damping ratios are neglected. The dynamic analysis of the adjacent structures linked by the optimized fluid damper under the white-noise ground excitation demonstrates that the modal damping ratios of the adjacent structures with the optimized fluid damper are considerably increased and the relative displacement responses of both the structures to the ground are significantly reduced. With either the optimization criterion, the control effectiveness of the damper increases as the difference of the natural frequencies of the two structures increases. There is an optimum mass ratio, by which the response of the structure is minimized. However, when the natural frequencies of the two structures are very close to each other, the damper has no function.

The fluid damper of the optimum parameters determined from the analytical formulas have also been applied to link the adjacent structures subjected to either the filtered white-noise ground excitation or the El Centro 1940 NS earthquake to examine the applicability of the analytical formulas to practical problems. The results from three pairs of example adjacent structures manifest that the optimum parameters determined from the analytical formulas are also beneficial to reduce the responses of the adjacent structures under either the filtered white-noise ground excitation or the real earthquake excitation. However, it is noticed that there are some cases in which the response reduction of the adjacent structures is small because either the dominant excitation frequency is far away from the natural frequency of the structure or the installation of the fluid damper makes the frequency of the structure more close to the dominant excitation frequency. Also in some cases, the response reduction of the adjacent structures under the El Centro ground excitation is moderately smaller than that under the white-noise ground excitation or the filtered white-noise ground excitation.

Acknowledgements

The writers are grateful for the financial support from the Hong Kong Polytechnic University through its Area of Strategic Development Program in Structural Control and Intelligent

Buildings. The joint support from the National Natural Science Foundation of China (NSFC 50378041) and the Excellent Young Teachers Program of the Ministry of Education of China to the second writer is also greatly appreciated.

References

[1] K. Gurley, A. Kareem, L.A. Bergman, E.A. Johnson, R.E. Klein, Coupling tall buildings for control of response to wind, *Proceedings of the Sixth International Conference on Structural Safety and Reliability* (*ISOSSAR*), A.A. Balkema, Rotterdam, 1994, pp. 1553–1560.
[2] J.E. Luco, C.P. De Barros, Optimal damping between two adjacent elastic structures, *Earthquake Engineering and Structural Dynamics* 27 (1998) 649–659.
[3] K. Iwanami, K. Suzuki, K. Seto, Studies of the vibration control method of parallel structures, *Transactions of JSME*, *No. 86-0247A*, 1986, pp. 3063–3072.
[4] W.S. Zhang, Y.L. Xu, Dynamic characteristics and seismic response of adjacent buildings linked by discrete dampers, *Earthquake Engineering and Structural Dynamics* 28 (1999) 1163–1185.
[5] G.B. Warburton, Optimum absorber parameters for various combination of response and excitation parameters, *Earthquake Engineering and Structural Dynamics* 10 (3) (1982) 381–401.
[6] M.Q. Feng, A. Mita, Vibration control of tall buildings using mega-subconfiguration, *Journal of Engineering Mechanics, American Society of Civil Engineers* 12 (10) (1995) 1082–1088.
[7] H.P. Zhu, H. Iemura, A study of response control on the passive coupling element between parallel structures, *Structural Engineering and Mechanics* 9 (4) (2000) 383–396.
[8] M.C. Constantinou, M.D. Symans, Experimental study of seismic response of buildings with supplemental fluid dampers, *Structural Design of Tall Buildings* 2 (1993) 93–132.
[9] T.T. Soong, G.F. Dargush, *Passive Energy Dissipation System in Structural Engineering*, Wiley, Chichester, 1997.
[10] W.S. Zhang, Y.K. Xu, Vibration analysis of two buildings linked by Maxwell model-defined fluid dampers, *Journal of Sound and Vibration* 233 (5) (2000) 775–796.
[11] R.B. Bird, R.C. Armstrong, O. Hassager, *Dynamics of Polymeric Liquids*, Wiley, New York, 1987.
[12] L. Cremer, M. Heckl, *Structure Borne Sound*, Springer, New York, 1973.
[13] H.M. James, N.B. Nichols, R.S. Phillips, *Theory of Servo Mechanisms*, McGraw-Hill, New York, 1947.
[14] J.C. Hayen, W.D. Iwan, Response control of structural systems using active interface damping, *Proceedings of the First World Conference on Structural Control*, Vol. 1, Los Angeles, CA, 1994, pp. 23–32.
[15] G.W. Housner, Properties of strong ground motion earthquakes, *Bulletin of Seismological Society of America* 53 (3) (1955) 197–218.
[16] Y.K. Lin, Y. Yan, Evolutionary Kanai-Majimi earthquake models, *Journal of Engineering Mechanics, American Society of Civil Engineers* 113 (8) (1987) 197–218.
[17] R.W. Clough, J. Penzien, *Dynamics of Structures*, McGraw-Hill, New York, 1975.
[18] H. Tomohiko, K. Takuji, I. Masatoshi, N. Naoki, Dynamic analysis of structures with Maxwell model, *Earthquake Engineering and Structural Dynamics* 29 (2000) 159–176.